Multiple Photocycles of Channelrhodopsin

Peter Hegemann,* Sabine Ehlenbeck,* and Dietrich Gradmann†
*Experimentelle Biophysik, Fachbereich für Biologie, Humboldt-Universität zu Berlin, 10115 Berlin, Germany; and †Albrecht-von-Haller-Institut für Pflanzenwissenschaften der Universität, 37073 Göttingen, Germany

ABSTRACT Two rhodopsins with intrinsic ion conductance have been identified recently in *Chlamydomonas reinhardtii*. They were named "channelrhodopsins" ChR1 and ChR2. Both were expressed in *Xenopus laevis* oocytes, and their properties were studied qualitatively by two electrode voltage clamp techniques. ChR1 is specific for H^+, whereas ChR2 conducts Na^+, K^+, Ca^{2+}, and guanidinium. ChR2 responds to the onset of light with a peak conductance, followed by a smaller steady-state conductance. Upon a second stimulation, the peak is smaller and recovers to full size faster at high external pH. ChR1 was reported to respond with a steady-state conductance only but is demonstrated here to have a peak conductance at high light intensities too. We analyzed quantitatively the light-induced conductance of ChR1 and developed a reaction scheme that describes the photocurrent kinetics at various light conditions. ChR1 exists in two dark states, D1 and D2, that photoisomerize to the conducting states M1 and M2, respectively. Dark-adapted ChR1 is completely arrested in D1. M1 converts into D1 within milliseconds but, in addition, equilibrates with the second conducting state M2 that decays to the second dark state D2. Thus, light-adapted ChR1 represents a mixture of D1 and D2. D2 thermally reconverts to D1 in minutes, i.e., much slower than any reaction of the two photocycles.

INTRODUCTION

Algal eyes contain several rhodopsins that control phototaxis and photophobic responses for finding good growth conditions. Two rhodopsin-like proteins (Chlamyrhodopsin-1 and Chlamyrhodopsin-2) were purified from algal eyes. They show sequence homology to animal rhodopsins but are not involved in behavioral responses (1). Later, two microbial-type rhodopsin sequences were identified as expressed sequence tags from the genome project. Expression of these rhodopsins in *Xenopus laevis* oocytes revealed that both operate as light-activated ion channels (2,3). Since they represent a new class of sensory photoreceptors and a new rhodopsin family, they were named channelrhodopsin-1 (ChR1) and channelrhodopsin-2 (ChR2). Depletion of ChR1 and ChR2 in *Chlamydomonas reinhardtii* by RNA_i reduced the photocurrents measured at high light intensities, suggesting that both channelrhodopsins are involved in behavioral responses (4). However, their specific role for phobic responses and phototaxis awaits further investigation.

For ChR1, only currents in response to light pulses of some 100 ms and high light intensities (500 nm, $>10^{21}$ photons m^{-2} s^{-1}) were studied (2). After light-on, currents were reported to rise to a steady-state level within a few milliseconds. After light-off, the current decays biexponentially. ChR1 conducts exclusively H^+ as judged from coincidence of observed reversal voltage and the Nernstian H^+-equilibrium potential (2). ChR2 has been studied in more detail. The photocurrents of ChR2 recorded at $pH_o = 9$ point to a conductance of ChR2 for ions different from H^+ as well. In fact, ChR2 also conducts the physiologically relevant ions K^+ and Ca^{2+}. The conducting pore of ChR2 must be wider than that of ChR1 because even guanidinium and methylamine pass ChR2 (3). Opening of the ChR2 channel is also faster than 1 ms. Closing of ChR2 after light-off occurs with $\tau \approx 1$ s at $pH_i = 4$ and $\tau \approx 10$ ms at $pH_i = 8$ (3). Upon sudden exposure to continuous light, the initial peak decays biexponentially to the steady-state level. Application of a second light pulse results in smaller peak amplitudes but the same steady-state levels. Recovery of the transient has been probed by double-light pulses with different temporal distances but has not been systematically investigated yet. Nevertheless, it is clear that the recovery is faster at high pH_o and requires many seconds to several minutes depending on the particular conditions. This led to the suggestion that protonation of an extracellular amino acid side chain is rate limiting for in- and reactivation (3).

Here we present a more detailed study of ChR1-photocurrents, focusing on the kinetics of the currents under different light regimes. We demonstrate that upon light pulses of sufficient intensity, ChR1 also shows an initial peak before the steady-state conductance is established, as reported previously for ChR2 only. We present a quantitative kinetic analysis of ChR1 photocurrents with the main result that a single photocycle cannot describe the experimental data, but two cycles with connected conducting states do. The results show that not only spectroscopic approaches but also electrophysiological experiments are suitable to identify and analyze reaction cycle intermediates of channelrhodopsin.

MATERIALS AND METHODS

Expression of ChR2 in oocytes or mammalian cells

A full-length Chop1 (aa 1–737) and a C-terminally truncated Chop1 variant (Chop1-345; aa 1–345) were produced from full-length cDNA templates

Submitted July 6, 2005, and accepted for publication August 22, 2005.

Address reprint requests to Peter Hegemann, E-mail: hegemann@rz.hu-berlin.de.

0006-3495/05/12/3911/08 $2.00

doi: 10.1529/biophysj.105.069716

(accession No: AF385748) by polymerase chain reaction, using a proof-reading polymerase (pfu, Promega, Mannheim, Germany) with primers containing *Bam*HI and *Hin*dIII restriction sites. The products were inserted into pGEMRe2 and verified by sequencing. cRNAs were expressed in oocytes of *X. laevis* as previously described (2,3).

Oocytes were injected with 20–30 ng of in vitro transcribed cRNA (Ambion, Huntingdon, UK) and incubated for 2–5 days with all-*trans* retinal (1 μM, from a 1 mM stock in ethanol) in standard buffer (10 mM 3-(*N*-morpholino)propanesulfonic acid, 4 mM KCl, 96 mM NaCl, 1 mM $MgCl_2$, 2 mM $CaCl_2$). Oocytes were examined using two electrode voltage-clamp techniques (5). ChR1 was stimulated with a xenon arc lamp (75 W, Jena Optics, Jena, Germany) equipped with a 500 ± 25 nm band filter (K50, Balzers, Liechtenstein) and focused onto the oocyte using a 2 mm light guide. The photon irradiance at the light-exposed surface of the oocyte was 5 mW/mm^2, corresponding to 10^{21} photons m^{-2} s^{-1}, 100%). In our hands, both constructs led to an identical light-gated proton conductance. All experiments presented in the figures were carried out with ChR1-315.

Numerical methods

The custom-tailored software used here is written in Turbo Pascal and is available on request. For fitting the model parameters to the data, a simple least square routine was applied (6), which is slow but does not lead into side minima as frequently as faster gradient algorithms. In this routine, all parameter values are consecutively increased and decreased by a common, small increment (typically 1%), and the change, which results in a smaller sum of least squares, replaces the previous parameter value. Cycles of such decisions through all parameters are repeated. When the error function does not improve anymore, the increment is reduced (1/2) until it falls under a threshold (typically 0.01%) which serves as a stop criterion. Sets of start parameters were chosen by educated guesses according to the experimental data. Once such a set led to visually satisfying fits, alternative fits with start parameters that deviated in the range of factor 2 usually converged to equivalent numerical solutions—within statistical limits, of course.

RESULTS AND DISCUSSION

Experimental data

The cRNA-encoding amino acid 1–345 of cChR1 was injected into freshly prepared oocytes from *X. laevis*. After 2 days, photocurrents could be recorded that increased in size during the following 5 days. The records of Fig. 1 *a* show photocurrents of ChR1 from oocytes at pH_o 4 and a membrane voltage of −100 mV under two-electrode voltage-clamp conditions. Most obvious is the fact that photocurrents are graded over a wide range of light intensities. At saturating light pulses of 500 nm (100%: $\sim 3 \times 10^{20}$ photons m^{-2} s^{-1}) and pH 7, photocurrents were <100 nA but they reached up to 2 μA under acidic conditions like pH_o 4. Photocurrents were virtually independent of Na^+, K^+, Ca^{2+}, and Cl^- in the medium as reported by Nagel et al. (2). At light pulses of low to moderate intensity (500 nm, <2.5% intensity), photocurrents were stationary after some 10 ms. At higher light intensities the rise of the photocurrent becomes faster with $\tau < 1$ ms at saturating light and passes a peak before reaching the steady-state level (Fig. 1 *a*). This was unexpected since in earlier experiments a transient component of the activity has only been observed for ChR2 (3) but not for ChR1 (2). The peak activity decays biexponentially with a main τ-value (amplitude >80%) of ~30 ms at saturating light, i.e., faster than that of ChR2 ($\tau \sim 140$ ms) at −100 mV and pH 4 (S. Ehlenbeck, unpublished). At pH_o 4 both the transient and the stationary fraction of the ChR1 photocurrent saturate at lower light intensities if compared to photocurrents recorded at pH_o 6 and pH_o 7.6 (Fig. 1, *b* and *c*), indicating that the photocycle is slower under acidic conditions. Moreover, the transient fraction of the current at a given light intensity is smaller at acidic pH even if the dark periods between subsequent light pulses are long (>5 min).

After light-off, the current decays biexponentially with $\tau_1 \sim 15$ ms and $\tau_2 \sim 25$ ms. These relaxation times are about twice as fast as the decay times of the transient current component at saturating light. The current decay is independent of the light pulse intensity and the membrane voltage (−100 to +40 mV). The influence of intracellular pH on these relaxation lifetimes has not been tested.

After step-up light stimulation, in many experiments the stationary current slowly increased by ~10% after the end of the transient with a time constant of ~500 ms (Fig. 1 *a*). It is excluded that this slow rise is due to a background drift, because current records in response to simple voltage steps did not show this phenomenon and, moreover, such an increase never occurred in oocytes expressing ChR2 (Ehlenbeck, unpublished).

The response to a second light pulse shows equal stationary currents but reduced amplitudes of the transient component (Fig. 1 *d*). The reduction is more pronounced when the pause between the two light pulses is short. In contrast to ChR2, the decay of the ChR1 currents is almost independent of the membrane voltage (between −100 and +40 mV) (data not shown).

Kinetic model for the description of the observed photocurrents

The temporal behavior of a unidirectional *n*-state reaction cycle with occupancies p_1–p_n is described by a set of p_i start occupancies, a set of rate constants, $k_{i,i+1}$ representing the transition probabilities from one state to the next, and the changes

$$\Delta p_i = (k_{i-1,i}\, p_{i-1} - k_{i,i+1} p_i)\Delta t \qquad (1)$$

for small time increments Δt, with $i = 1$ to n and $i - 1 = n$ if $i = 1$.

Transitions between specific states of more than one cycle can be formulated correspondingly. For the purpose of this study, the assignment of the indices and states in the reaction cycles of Fig. 2 is D = 1, K = 2, L = 3, etc. Start conditions in the dark are defined by $p_1 = 1$ and $p_{>1} = 0$. Light enters the system by the light-sensitive rate constant $k_{12} = k_{12}^0 \times$ light, where k_{12}^0 is k_{12} at a half saturating reference light intensity (photon irradiance) of $\sim 8 \times 10^{19}$ photons m^{-2} s^{-1} (at an absorption cross section σ of 1.2×10^{-20} m^{-2}).

It is clear that immediately after the light pulse with all $k > 0$ except $k_{12} = 0$ (light-off conditions), the system will

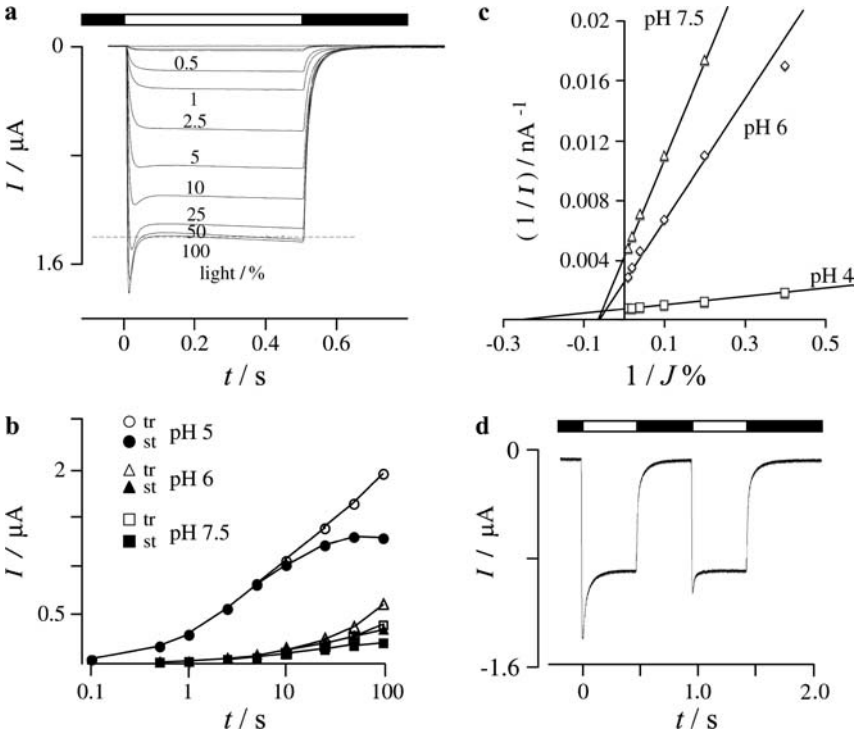

FIGURE 1 (*a*) ChR1 photocurrents recorded at pH_o 4 and −100 mV and light pulses of 500 nm and various intensities indicated in percentages. 100% corresponds to 3×10^{20} photons m^{-2} s^{-1}. The illumination period is indicated by a horizontal bar above the current traces. (*b*) Amplitudes of the peak currents (*open symbols*) and the stationary currents (*solid symbols*) measured 200 ms after light-on recorded at pH 7.5, 6, and 5 plotted versus the intensity of the actinic light. Other conditions were as under *a*. (*c*) Plot of the reciprocal amplitudes of the stationary currents versus the reciprocal light intensity. (*d*) Typical trace in response to double light-pulse stimulation (100% green light).

approach $p_i = 0$ except $p_1 = 1$. For a numerical description of the observed photocurrents on the basis of the reaction kinetic model of Fig. 2, *e* and *f*, we used the following rearranged differential equations:

$$\Delta p_{D1} = (-k_{DM1}p_{D1} + k_{MD1}p_{M1} + k_{D21}p_{D2})\Delta t \quad (1a)$$

$$\Delta p_{D2} = (-(k_{D21} + k_{DM2})p_{D2} + k_{MD21}p_{M2})\Delta t \quad (1b)$$

$$\Delta p_{M1} = (-(k_{M12} + k_{MD1})p_{M1} + k_{DM1}p_{D1} + k_{M21}p_{M2})\Delta t \quad (1c)$$

$$\Delta p_{M2} = (-(k_{M21} + k_{MD2})p_{M2} + k_{DM2}p_{D2} + k_{M12}p_{M1})\Delta t, \quad (1d)$$

with the four probabilities p_i of the occupancy of the indicated states and the indicated transition probabilities k_{ij} from state *i* to state *j*.

Before illumination, all *p* values are zero except $p_{D1} = 1$ of the ground state, because of $k_{DM1,2} = 0$ and $k_{D12} = 0$. Upon the onset of continuous light, $k_{DM1,2}$ are > 0, which causes the four occupancies p_i to change by Δp_i within a short time interval Δt.

By these means, the time courses of p_i (k, t) can be calculated iteratively

$$p_{i,t} + \Delta t = p_{i,t} + \Delta p_i \quad (2)$$

for any light protocol. Currents (I) are obtained by assigning ion transport functions $I_i(c,V)$ to the individual states (c: internal and external substrate concentrations, V: transmembrane voltage):

$$I = \Sigma(p_i I_i). \quad (3)$$

Here, all transport functions are assumed to be zero, except for the M-states to which the simple ohmic relationship

$$I_M = g_M V, \quad (4)$$

is assigned.

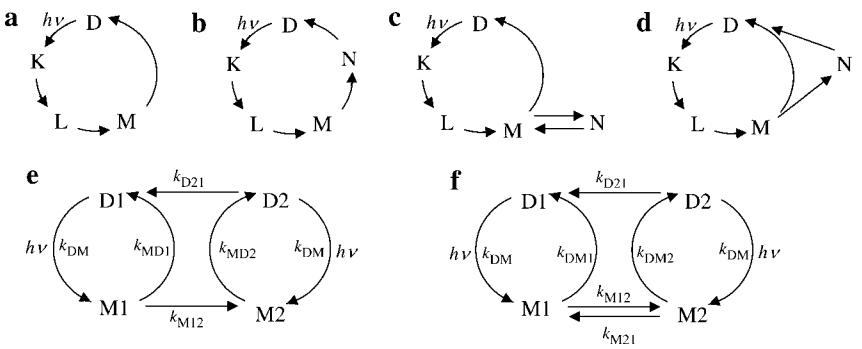

FIGURE 2 Photocycle models that were tested with respect to describing the ChR1 photocurrents. Cycles *b–d* could explain the fast transient current component but not simultaneously the slow recovery in the dark. Cycles *e* and *f* may in addition explain the slow recovery of the photocurrents as a slow back reaction from D2 to D1.

The proposed model corresponds to the following knowledge

All microbial-type rhodopsins undergo a cyclic sequence of reactions (photocycle) and do not need a second photon or enzymatic activities for the recovery of the dark state as mammalian rhodopsins do. All rhodopsin photocycles start with the absorption of light followed by excitation of the retinal chromophore from an electronic ground state, S0 (dark form), to an electronically excited state, Sn. Excited states with Sn $>$ 1 are deactivated to S1 or S0 within 1 ps without significant conformational change. During the lifetime of S1 the electronic distribution within the retinal chromophore changes, causing a minor motion of the retinal relative to protein environment. This is regarded as the initiation of a rotation around the 11-12 bond in animal rhodopsins or 13-14 bond in microbial rhodopsins. Channelrhodopsins are likely to isomerize around the 13-14 bond since channelrhodopsins comprise an archaeen-type retinal-binding pocket (4,7), mainly all-*trans* retinal was extracted from *Chlamydomonas* cells (8—10) and in oocytes channelrhodopsins are rapidly reconstituted with all-*trans* retinal. To achieve a high quantum efficiency, full retinal isomerization must be reached within a few picoseconds (11) on the way from the relaxed excited state to the first ground state of the photocycle. Such an early fully isomerized electronic ground state is named K intermediate. This hot K-state relaxes on a nanosecond timescale to the next more-relaxed product named L-state as derived from the animal rhodopsin photoproduct *Lumi*. Since photocurrents do not occur within nanoseconds, only the third photocycle intermediate is a possible conducting state. Thus we named the conducting state M-state in analogy to the signaling metastates of other rhodopsins (12). Such a simple photocycle (*circle a* in Fig. 2) may explain flash-induced photocurrent transients and steady-state photocurrents as they occur during long light pulses.

Compatibility of the observed photocurrents with photocycle models

Although the photocycle in Fig. 2 *a* is most suggestive, it cannot explain the observed relaxation of the photocurrents from a peak to a lower steady-state level in continuous light. Therefore we have suggested before that a less conducting state, M2, or a nonconducting state, N, had to be included in the cycle (3). Such a low conductance state may follow the M-state as a consecutive state before it decays into the dark state, D (Fig. 2 *b*). In this cycle k_{ND} should be of the same order as k_{MN} to explain conductance relaxation to ~3/4–2/3 of the peak current depending on the pH. Alternatively, the low conducting or nonconducting state may reflect a side reaction of M as seen in Fig. 2 *c*. Such a cycle has been proposed for halorhodopsin that deprotonates at high light levels more slowly than the kinetics of the transport cycle (13) and for bacteriorhodopsin on the basis of electrical measurements on black lipid membranes to explain accumulation of the M-intermediates at negative membrane voltage (14). For channelrhodopsins k_{NM} must be in the range of 0.01 s^{-1} to explain a recovery within minutes. And second, k_{MN} and k_{NM} must be of the same order to prevent complete bleaching. But, if k_{MN} is small the photocurrent transient would have slower decay kinetics than is actually observed. It might be assumed that the latter obstacle is prevented by a reaction from N directly back to D (Fig. 2 *d*). But again, k_{ND} cannot be much smaller than k_{MN} to avoid complete inactivation in continuous light. Thus, none of the reaction cycles in Fig. 2, *a–d*, can explain the major properties of the observed photocurrents, namely, the fast decay of the transient, the size relation of the transient and the stationary photocurrent, the fast decay of the photocurrent after light-off, and the slow recovery of the transient (dark adaptation). Since the discrepancy between the photocycles of Fig. 2, *a–d*, and the data are of a systematic nature, a quantitative evaluation seemed not to be useful.

To our understanding, the sum of all observations can only be explained by a second conducting state, M2, that is populated from both the conducting state, M1, and from a second dark state, D2 (Fig. 2 *e*). Since the D $\rightarrow$ K and K $\rightarrow$ L transitions are too fast for our simulation (15) and too fast for recording in oocytes, the transitions D $\rightarrow$ K $\rightarrow$ L $\rightarrow$ M have been combined into the D $\rightarrow$ M transition. M1 and M2 decay within milliseconds, whereas the thermal conversion of D2 to D1 requires $>$10 s. D1 $\rightarrow$ M1 and D2 $\rightarrow$ M2 are assumed to be equal, resulting in a 2 $\times$ 2 state model with only five independent rate constants. This model accounted for the described phenomena quite well. It provides the rate constants by unambiguous fits of the model system to the experimental data.

The fit of the model to a response of a double light pulse at pH 5 is shown in Fig. 3 *a*. The rise of the current, the decay of the transient, and the stationary current are well represented. The reduced size of the second transient is only qualitatively reflected. Also the late decay of the current after light-off is not perfectly described and demands a more complex model (see below). The numerical values of the fitted rate constants for all transitions are listed in the legend to Fig. 3 *a*. Fig. 3 *b* shows the calculated occupancy probabilities ($0 < p < 1$) of the photocycle intermediates D1, M1, D2, and M2, using rate constants in such a way that the occupancies of M1 + 1/2 M2 are proportional to the current observed at pH_o 5. This means that the conductance of M2 is ~½ of the M1 conductance (based on model 2 *e*).

The slow rise of the stationary ChR1 current (see *dashed line* in Fig. 1 *a*) is not explained by the four-state model of Fig. 2 *e*. Introduction of an additional, nonconducting state, N1, into the photocycle between the states M1 and D1 is able to account for this observation in principle (details not shown). Such a late N-state is seen in archaean-type rhodopsins under acidic conditions when the reaction of M to N/O is fast. If the late N-state decays slowly, it is significantly populated shortly after light-on. When the illumination time is

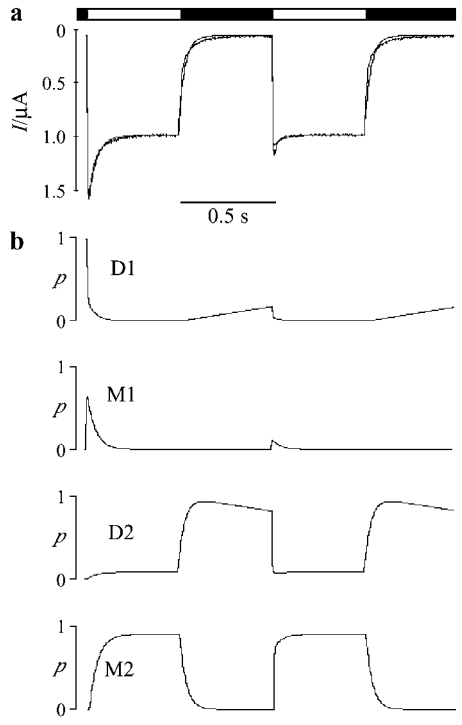

FIGURE 3 (*a*) Recorded photocurrents to double pulse stimulation (*noisy tracing*) and fit (*smooth tracing*) using the 2 × 2 state model of Fig. 2 *e*. The rate constants of the theoretical curve with initial, rounded parameter values are $k_{DM1} = k_{DM2} = 369\ s^{-1}$ at $\sim 10^{21}$ photons $m^{-2}\ s^{-1}$ irradiance, $k_{MD1} = 108\ s^{-1}$, $k_{MD2} = 36\ s^{-1}$, $k_{M12} = 31\ s^{-1}$, $k_{M21} = 0\ s^{-1}$, $k_{D21} = 0.4\ s^{-1}$, $G_1 = 22.3$ nS, and $G_2 = 10.6$ nS. (*b*) Calculated concentrations of the photocycle intermediates D1, M1, D2, and M2.

progressing, an increasing number of molecules will not operate through cycle 1, but cycle 2 and depopulation of D1 will be seen as a reduction of the conductance. Residual molecules arrested in N1 only slowly cycle through M1 from where they convert to M2, seen as a slow rise of the current (data not shown). Since this complication is not needed to explain photocurrents seen under most experimental conditions, the kinetic effects of such additional intermediates are not treated here explicitly.

Dark adaptation

The reaction scheme of Fig. 2 *e* predicts the slow recovery of D1 as a single exponential. However, when the dark period between two light pulses was varied systematically, the recovery turned out to consist of a fast and a slow component that could be fitted by two exponentials: Recovery $= A_1 \times \exp(-t/\tau_1) + A_2 \times \exp(-t/\tau_2)$, where A_1 and A_2 are the portions of the fast and slow components ($A_1 + A_2 = 1$). Fits to the results from three different pH_o are illustrated in Fig. 4 *a*. The fitted values of τ_1, τ_2, and $A_{1,2}$ from several experiments are plotted versus pH_o in Fig. 4, *b*, *c*, and *d*, respectively. Recorded changes of τ_1 are neither significant nor important at this place.

In contrast, τ_2 and $A_{1,2}$ vary significantly upon acidification (Fig. 4, *c* and *d*). The biexponential recovery, in particular the slow component, cannot be explained by any model in Fig. 2. It can be described, however, by introduction of a third D state, D3, which slowly equilibrates with D2, as illustrated in the reaction scheme of Fig. 4 *f*.

Based on the performed calculations, D3 can be assumed to have the same photochemical properties as D2 ($k_{DM3} = k_{DM2}$, $k_{MD3} = k_{MD2}$, $G_{M3} = G_{M2}$), which renders the description of an individual double pulse response independent of this extension. In such a system, the dark state, D1, will recover with $D1(t) = A_1 \times \exp(-t/\tau_1) + A_2 \times \exp(-t/\tau_2)$, where the three independent observables τ_1, τ_2, and A_1 ($A_2 = 1 - A_1$ is not independent) correspond to the three system parameters k_{D32}, k_{D23}, and k_{D21} by the relationships $1/\tau_1 + 1/\tau_2 = k_{D32} + k_{D23} + k_{D21}$, $1/(\tau_1 \times \tau_2) = k_{D32} \times k_{D21}$, and $A_1 = k_{D32}/(k_{D23} + k_{D32})$. In our case, when τ_1 and τ_2 differ by ~ 2 orders of magnitude, the τ values can be approximated by the simpler relationships $1/\tau_1 = k_{D21}$, and $1/\tau_2 = k_{D23} + k_{D32}$. Thus the three independent system parameters can be expressed by the three observables as $k_{D21} = 1/\tau_1$, $k_{D23} = A_2/\tau_2$, and $k_{D32} = 1/\tau_2 - k_{D23}$. Using averaged data of the observables (*solid points* in Figs. 4, *b–d*), the system parameters are plotted versus pH_o in Fig. 4: the trivial $k_{D21} = 1/\tau_1$ in panel *b* (*solid points*) and the nontrivial k_{D23} and k_{D32} in Fig. 4 *e*. These results can be summarized by the assessment that the biphasic recovery and its pH_o sensitivity are well described by the reaction scheme in Fig. 4 *f* with pH_o-insensitive $k_{D21} \approx 3\ s^{-1}$ and $k_{D23} \approx 0.007\ s^{-1}$ and a pH_o-sensitive k_{D32} rising from $0.002\ s^{-1}$ at pH_o 5 over $0.007\ s^{-1}$ at pH_o 6 to $0.008\ s^{-1}$ at pH_o 7.5. The mechanism of this pH_o sensitivity of k_{D32} is not known.

Modeling responses to light pulses of different intensity

We have found that the transient fraction of photocurrents recorded at pH 4 is quite variable, as caused by the slow recovery of D1 under acidic conditions. Already dim light or even repetitive flashing with a frequency of >0.001 Hz were causing significant light adaptation seen as reduction of the current transient. Therefore, we concentrated on the simulation of photocurrent measurements at $pH_o = 5$. Fig. 5 *a* shows fits to recordings with 100%, 25%, and 10% light. One set of rate constants is sufficient for describing all the stationary levels and transients quite well. However, the relative amplitudes of the transients are too large and the kinetics of the transient for nonsaturating light intensities is not adequately taken into account. Thus, we needed a modification of the four-state model of Fig. 2 *e* that results in a smaller dynamic range of the transient and a narrow range for the transient kinetics. One option was to make the transition M1 to M2 light dependent, rendering the reactions from D1 to M2 a two-photon process. This can explain why ChR1 only exhibits transients at high light intensities as seen

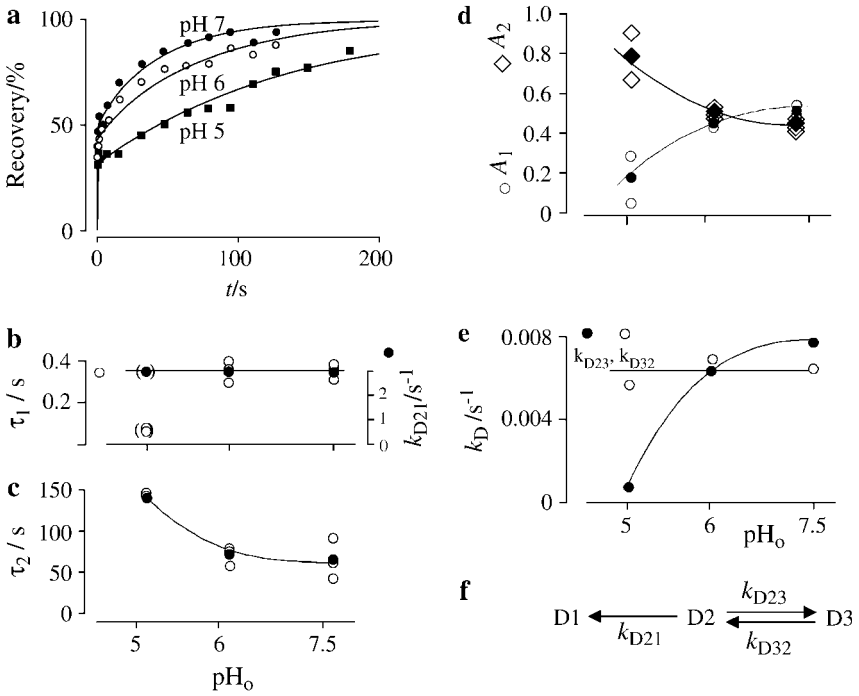

FIGURE 4 Recovery of the transient current component at variable dark periods between two light pulses. (*a*) The recovery of the transient current ($I_{transient1}/I_{transient2}$) is plotted versus the dark period between the different light pulses (0.5 s each). The recovery is a biexponential process. (*b*) The measured τ_1-value (○) and the corresponding k_{D21} (●) are plotted versus pH_o and show no significant pHo sensitivity. The values at pH 5 are inconsistent. (*c*) Measured τ_2-values are plotted versus pH_o. Solid circles are averaged values. (*d*) Amplitudes of fast (A_1, *circles*) and slow (A_2, *diamonds*) components plotted versus pH_o; averaged values are seen as solid symbols. (*e*) Calculated rate constants k_{D23} and k_{D32} are plotted versus pH_o. (*f*) A model with three dark states that is consistent with the dark-adaptation process. D2 and D3 are in equilibrium, whereas D2 and D1 are not.

in Fig. 5 *b*. However, the shape of the transient becomes light dependent (between 10% and 100% saturation), a phenomenon not observed experimentally.

An alternative approach was the introduction of a back reaction from M2 to M1, thus establishing an equilibrium M1 ↔ M2 (model Fig. 2 *f*). As seen from the fit in Fig. 5 *c*, the dynamic range of the transient is small as requested, the location of the transient maxima is quite appropriate also at moderate intensities, and the stationary levels are well described. The optimal fit was achieved for a conductance ratio G_{M1}/G_{M2} of ~3:1. The qualitative difference between photocycles with and without M1 ↔ M2 equilibrium is that in case of equilibrium only 2/3 of the molecules are in the D2 cycle under fully light-adapted conditions. The ratio is defined by the ratio k_{M12}/k_{M21}. Fig. 5 *d* shows the fit of recordings to six different light intensities. Certainly, the fit to any individual recording is of lower quality, but qualitatively all individual curves are well represented by one set of system parameters. At low light, the real rise of the current is faster than that in the model. But, especially at low light the low optical transparency of the oocytes with uneven illumination of the rhodopsins has to be taken into account. Introduction of the back reaction improves the description of the transition from the peak to the steady-state level. In particular, without k_{M21}, the sharpness of the peaks grows much faster with the light intensity than in the experimental data.

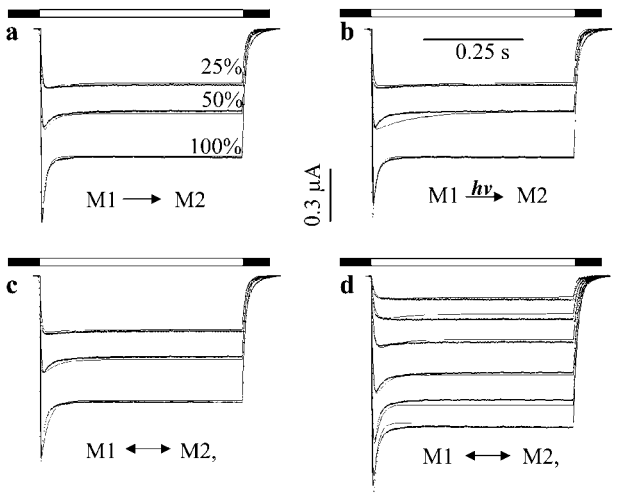

FIGURE 5 Photocurrents measured in response to light pulses of different intensities at pH 5 and fits generated on the basis of different model version. (*a*) 2 × 2 model of Fig. 2 *e*. (*b*) 2 × 2 model but with the M1 → −M2 transition defined as a light-dependent reaction. (*c*) 2 × 2 model including an M1 ↔ M2 equilibrium (Fig. 2 *f*). (*d*) Currents measured at six different intensities (100%, 50%, 25%, 10%, 5%, 2.5%). Calculated currents are seen as smooth lines. Parameter values of the best fit for the six curves in panel *d*: $k_{DM1} = 337\ s^{-1}$ and $k_{DM2} = 240\ s^{-1}$ at 100% green light of 3×10^{20} photons $m^{-2}\ s^{-1}$, $k_{MD1} = 75\ s^{-1}$, $k_{MD2} = 17\ s^{-1}$, $k_{M12} = 16\ s^{-1}$, $k_{M21} = 19\ s^{-1}$, k_{D21} not determined, $G_1 = 5.9$ nS, and $G_2 = 1.4$ nS. The light period is indicated above the current traces.

Evaluation of the four-state model

To evaluate the kinetic description of the ChR1 photocycle, we explicitly tested changes of the calculated photocurrents on the basis of the extended 2 × 2 state model of Fig. 2 *f* by specific variation of selected parameters and keeping all other parameters constant. We started with a reference system that optimally describes photoresponses to two subsequent light pulses at pH 6 (Fig. 6 *a*). Increase of the

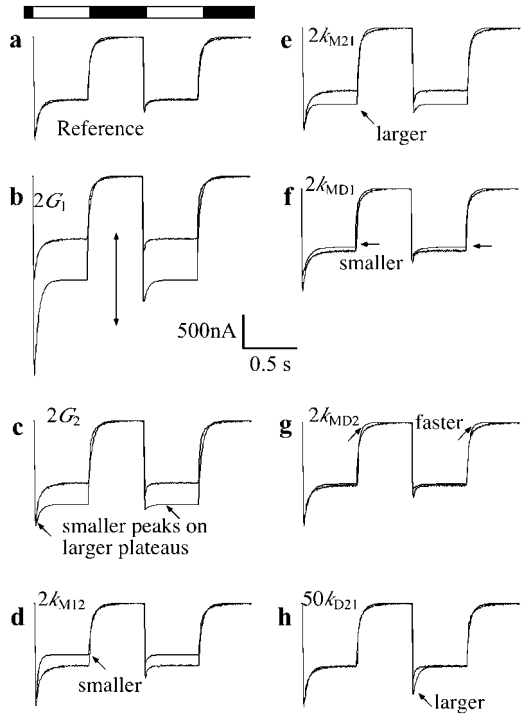

FIGURE 6 Specific influence of each model parameter on shape of current records in double light-pulse experiment, expressed as discrepancy between experimental data (*noisy tracing*) and theoretical record (*smooth tracing*) with changes of individual parameters as marked. (*a*) Reference fit with all parameters optimized: $k_{DM1} = k_{DM2} = 380\ s^{-1}$ at $\sim 10^{21}$ photons $m^{-2}\ s^{-1}$ irradiance, $k_{MD1} = 64\ s^{-1}$, $k_{MD2} = 14\ s^{-1}$, $k_{M12} = 14\ s^{-1}$, $k_{M21} = 9\ s^{-1}$, $k_{D21} = 0.03\ s^{-1}$, $G_1 = 19$ nS, and $G_2 = 5$ nS. *b–h*: Influence of parameters as marked.

conductance G_1 has a larger relative influence on the transient current component compared to that on the stationary current (Fig. 6 *b*), because G2 strongly contributes to the latter but not to the transient. Consequently, doubling G_2 increases the stationary fraction with concomitant reduction of the transient current (Fig. 6 *c*). Increasing k_{DM} twofold led to sharper transients, larger stationary currents, and a reduced ratio of P2/P1 (data not shown). Two times larger k_{M12} accelerates the current transients by accelerating the transition to the lower conducting state, whereas the size of the transient remains almost unchanged (Fig. 6 *d*). Due to the shifted M1 ↔ M2 equilibrium, the stationary conductance is also reduced. Consequently, increase of k_{M21} accelerates the transient decay and increased the stationary fraction (Fig. 6 *e*). The decay rate of M1 is more critical for the observed current than that of M2. Enhancement of k_{MD1} decreases the transient and the stationary current (Fig. 6 *f*), whereas the influence of k_{MD2} was only obvious with respect to the size of the second transient and the slow decay kinetics of the current after light-off (Fig. 6 *g*). In double flash experiments with short dark periods between the light pulses, the influence of k_{D21} becomes visible only when it was drastically enlarged (50× in Fig. 6 *h*). The second transient becomes larger, whereas all other features of the currents remain completely unchanged.

CONCLUSIONS

We have demonstrated above that the ChR1 photocurrents as they are recorded from *X. laevis* oocytes can be reliably described on the basis of two photocycles but not by only one. The cycles are connected via their conducting states, M1 and M2, as well as through the dark states D1 and D2. This 2 × 2 state model explains the observed light dependence of the photocurrents including that of the transient fraction. Additionally, it explains the reduction of the transient upon repetitive stimulation as well as the recovery during longer dark periods. This behavior is considered light adaptation and dark adaptation of ChR1. For the description of the biphasic dark adaptation, we discussed a third protein subspecies with dark state and signaling state (D3 and M3) that are kinetically connected to D2 and M2, respectively.

We thank Drs. George Nagel, Rolf Hagedorn, and Chris Kay for discussion, suggestions, and technical support.

This work was supported by the Deutsche Forschungsgemeinschaft (P.H.).

REFERENCES

1. Fuhrmann, M., E. Govorunova, S. Rank, and P. Hegemann. 2001. The dominant retinal protein of the *C. reinhardtii* eye is not the photoreceptor for phototaxis. *J. Cell Sci.* 114:3857–3862.
2. Nagel, G., D. Ollig, M. Fuhrmann, S. Kateriya, A.-M. Musti, E. Bamberg, and P. Hegemann. 2002. Channelrhodopsin-1, a light-gated proton channel in green algae. *Science*. 296:2395–2398.
3. Nagel, G., T. Szellas, W. Huhn, S. Kateriya, N. Adeishvilli, P. Berthold, D. Ollig, P. Hegemann, and E. Bamberg. 2003. Channelrhodopsin-2, a light-gated cation channel in green algae. *Proc. Natl. Acad. Sci USA*. 100:13940–13945.
4. Sineshchekov, O. A., K.-H. Jung, and J. L. Spudich. 2002. Two rhodopsins mediate phototaxis in low and high intensity light in *Chlamydomonas reinhardtii*. *Proc. Natl. Acad. Sci. USA*. 99:8689–8694.
5. Stühmer, W. 1998. Electrophysiologic recording from *Xenopus* oocytes. *Methods Enzymol*. 293:280–300.
6. Hookes, R., and T. Jeeves. 1961. Direct search solution of numerical and statistical problems. *J. Assoc. Comput. Mach.* 8:212–229.
7. Kateriya, S., G. Nagel, E. Bamberg, and P. Hegemann. 2004. ''Vision'' in single-celled algae. *News Physiol. Sci*. 19:133–137.
8. Uhl, R., and P. Hegemann. 1990. Probing visual transduction in a plant cell. Optical recording of rhodopsin induced structural changes from *Chlamydomonas*. *Biophys. J*. 558:1295–1302.
9. Beckmann, M., and P. Hegemann. 1991. In vitro identification of rhodopsin in the green alga *Chlamydomonas*. *Biochemistry*. 30:3692–3697.
10. Takahashi, T., K. Yoshihara, M. Watanabe, M. Kubota, R. Johnson, F. Derguini, and K. Nakanishi. 1991. Photoisomerization of retinal at 13-ene is important for phototaxis of Chlamydomonas reinhardtii: simultaneous measurements of phototactic and photophobic responses. *Biochem. Biophys. Res. Commun*. 178:1273–1279.
11. González-Luque, R., M. Garavelli, F. Bernardi, M. Merchán, M. A. Robb, and M. Olivucci. 2000. Computational evidence in favor of a two-state, two-mode model of the retinal chromophore photoisomerization. *Proc. Acad. Natl. Acad. Sci. USA*. 97:9379–9384.

12. Okada, T., O. P. Ernst, K. Palczewski, and K. P. Hofmann. 2001. Activation of rhodopsin: new insights from structural and biochemical studies. *Trends Biochem. Sci.* 26:318–324.

13. Hegemann, P., D. Oesterhelt, and M. Steiner. 1985. The photocycle of the chloride pump halorhodopsin, I. Azide catalysed deprotonation of the chromophore is a side reaction of the photocycle intermediates inactivating the pump. *EMBO J.* 4:2347–2350.

14. Geibel, S., T. Friedrich, P. Ormos, P. Wood, G. Nagel, and E. Bamberg. 2001. The voltage-dependent proton pumping in bacteriorhodopsin is characterized by optoelectric behavior. *Biophys. J.* 81: 2059–2068.

15. Lozier, R. H., R. A. Bogomolni, and W. Stoekenius. 1975. Bacteriorhodopsin: a light-driven proton pump in *Halobacterium halobium*. *Biophys. J.* 15:955–962.